Star, L. M., Tileylioglu, S., Givens, M. J., Mylonakis, G., & Stewart, J. P. (2019). Evaluation of Soil-Structure Interaction Effects from System Identification of Structures Subject to Forced Vibration Tests. *Soil Dynamics and Earthquake Engineering*, *116*, 747-760. https://doi.org/10.1016/j.soildyn.2018.09.038

Evaluation of Soil-Structure Interaction Effects from System Identification of Structures Subject to Forced Vibration Tests

Lisa M. Star[a], Salih Tileylioglu[b], Michael J. Givens[c], George Mylonakis[d,e,f], and Jonathan P. Stewart[g]

[a] Corresponding Author. Assistant Professor, Department of Civil Engineering and Construction Management, California State University, Long Beach, 1250 Bellflower Blvd, Long Beach, CA 90850, U.S.A. lisa.star@csulb.edu
[b] Assistant Professor, Department of Civil Engineering, Cankaya University, Eskişehir Yolu 29.km 06810 Ankara/Turkey. saliht@cankaya.edu.tr
[c] Senior Engineer, Arup, 12777 W Jefferson Blvd # 200, Los Angeles, CA 90066. michael.givens@arup.com
[d] Professor, Department of Civil Engineering, University of Bristol, Bristol BS8 1TR U.K. G.Mylonakis@bristol.ac.uk
[e] Professor, Department of Civil Engineering, University of Patras, Panepistimioupoli Patron 265 04, Greece
[f] Adjunct Professor, Department of Civil and Environmental Engineering, University of California, Los Angeles, 420 Westwood Plaza, 5731 Boelter Hall, Los Angeles, CA 90095, U.S.A
[g] Professor, Department of Civil and Environmental Engineering, University of California, Los Angeles, 420 Westwood Plaza, 5731 Boelter Hall, Los Angeles, CA 90095, U.S.A. jstewart@seas.ucla.edu

1.0 ABSTRACT

We describe procedures to evaluate the dynamic properties of test structures subject to forced vibration testing. We seek modal vibration periods and damping ratios corresponding to the actual flexible-based response of the structure (incorporating the effects of compliance in the soil medium supporting the foundation) and similar attributes for a fixed-base condition in which only the flexibility of the structure is represented. Our approach consists of using suitable input and output time series with conventional parametric system identification procedures, and as such extends previously developed procedures for use with earthquake recordings. We verify the proposed approach and demonstrate its application using data from two test structures supported on shallow foundations that have been used in forced vibration tests and that have recorded earthquakes. The structures were tested with and without braces to modify their stiffness and were deployed at two sites with different soil conditions. We analyze the results to evaluate experimental period lengthening ratios and foundation damping. The results show (1) strong increases in period lengthening and foundation damping with the wave parameter (dimensionless ratio of structure-to-soil stiffness), (2) compatibility between modal properties from forced vibration testing and earthquake excitation, (3) soil nonlinearity increases period lengthening and modifies foundation damping in a manner that can be reasonably captured in predictive models using equivalent-linear soil properties compatible with a proposed shear strain index.

INTRODUCTION

System identification can be used to evaluate the unknown properties of a dynamic system using the observed input excitation applied to the system and the response of the system measured at selected locations. For applications to buildings, system identification can estimate modal frequencies, damping ratios, mode shapes, and other system properties [1] based on recorded system vibrations, typically at the roof and foundation levels. For investigations of Soil-Structure Interaction (SSI), it is useful to identify modal vibration parameters that describe the behavior of the superstructure only (fixed-base parameters) and the soil-foundation-structure system (flexible-base parameters). Fundamental-mode frequencies and damping ratios are distinct for the two base fixity conditions when the medium supporting the foundation is compliant.

For the case of earthquake excitation Stewart and Fenves [2] derived input and output data pairs required to evaluate fixed- and flexible-base modal parameters from system identification. The system considered is depicted in Figure 1(a) and the input-output pairs are listed in Table 1. In Figure 1, u_g represents the ground motion that would occur at the surface of the site if the building was not present, which is referred to as the free-field ground motion. By definition, free-field motions are unaffected by building vibrations. Motions u_f and θ_f represent the relative motions of the foundation base with respect to the free-field in translation and rotation, respectively, while u_s represents the relative translation of center of mass of the roof slab with respect to the base of the rotated foundation.

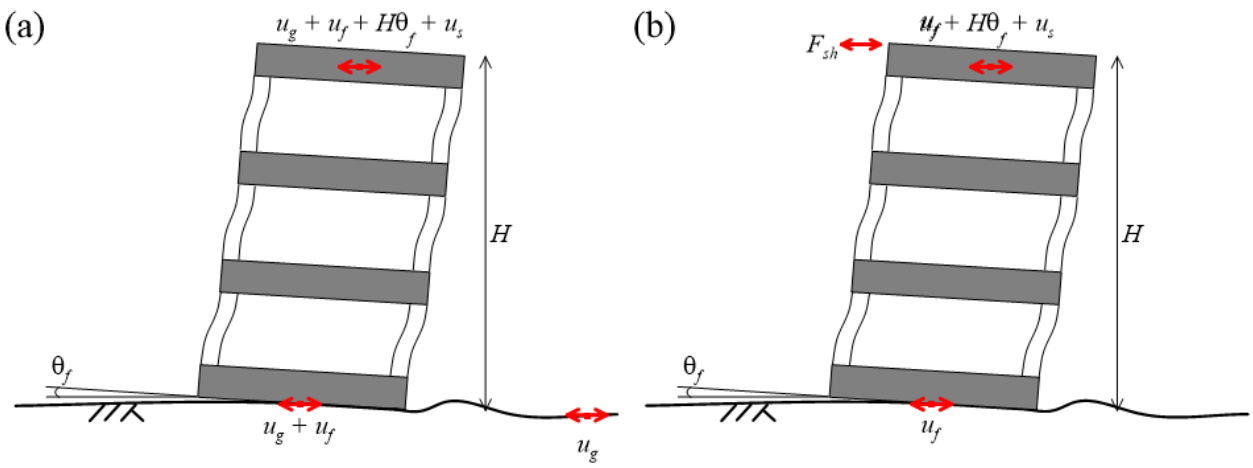

Fig 1. Recordings required for system ID with (a) earthquake excitation [2] and (b) forced vibration (this study)

Table 1. Input and output pairs from earthquake excitations for various base fixity conditions [2]. The motions are indicated as accelerations because the recorders used are typically accelerometers.

Base Fixity	Input	Output
Flexible-Base	$\ddot{u}_g$	$\ddot{u}_g + \ddot{u}_f + H\ddot{\theta} + \ddot{u}_s$
Pseudo Flexible-Base	$\ddot{u}_g + \ddot{u}_f$	$\ddot{u}_g + \ddot{u}_f + H\ddot{\theta} + \ddot{u}_s$
Fixed Base	$\ddot{u}_g + \ddot{u}_f + H\ddot{\theta}$	$\ddot{u}_g + \ddot{u}_f + H\ddot{\theta} + \ddot{u}_s$

We consider the case of excitation from forced vibration applied by a shaker mounted on the roof of a structure, as depicted in Figure 1(b). Many such experiments to evaluate vibration properties of structures have been performed (e.g., [3, 4, 5, 6, 7]). Applications of forced vibration testing in which the data interpretation considers SSI effects are relatively limited, but have been undertaken to investigate system performance and its predictability (e.g., Millikan library, [8]; Lotung and Hualien containment models, [9, 10], model structure [11]) and foundation impedance (Millikan library, [12]; model structures, [1, 13]). Luco et al. [12] developed two approaches to estimate fundamental-mode frequencies and damping ratios for the fixed-base condition using non-parametric system identification procedures, which is discussed further below. Those procedures are extended in Luco and de Barros [10] by applying parametric methods that estimate fixed base properties of the structure by fitting observed equivalent fixed-base displacements to equations for those displacements derived from theoretical models.

In this paper, we describe system identification procedures for evaluating fixed- and flexible-base modal properties of structures subject to forced vibration tests. There are two points of emphasis: (1) the system identification procedures themselves, for which we emphasize parametric approaches and (2) the input-output time series that are used, which are broadly applicable to multiple system identification approaches. Parametric procedures are emphasized here because they have some advantages relative to non-parametric procedures for SSI-related applications, including relatively direct quantification of damping. The distinctions between our approach and that of Luco and de Barros [10] are (1) our parametric optimization is based on transfer functions,

not fixed-base displacements and (2) we provide procedures for multiple base fixity conditions, not just fixed base.

Following this introduction, we review available system identification procedures and their suitability for analysis of structural properties for different base fixity conditions, and describe the parametric approach used in this paper. We then apply principles of structural dynamics to evaluate input-output time series for use with system identification procedures to evaluate fixed- and flexible-base fundamental mode vibration periods and damping ratios. We verify these input/output time series against numerical solutions and apply the proposed approach to data from forced vibration tests conducted on several model structures [14, 15]. The test results are used to evaluate inertial SSI effects (period lengthening and foundation damping) for comparison with predictions of models in engineering guidelines documents [16, 17]. The originality and significance of this work is related in part to the novelty of the system identification procedures that are described and demonstrated. Moreover, the test data that is presented significantly adds to the limited field performance data on SSI effects in the literature, which is needed for model validation purposes.

2.0 SYSTEM IDENTIFICATION METHODS

In their analysis of SSI effects from earthquake recordings, Stewart and Fenves [2] used ARX-type [18] parametric system identification procedures with alternate input/output time series. Here we consider whether this remains the appropriate choice given the many options for system identification in the literature, including methods published over the last two decades. We review available system identification procedures with an emphasis on their suitability for application to data from building structures.

Table 2 provides an overview of system identification methods. We organize this table into four families of methods consisting of two parametric, a non-parametric and newer approaches, as explained below. We identify the type of excitation each method is intended to be applied with, the main options being ambient noise, earthquake shaking, and forced vibration. We also identify whether the solution is formulated in the time- or frequency-domains. Where applicable, we provide references for application of the approach to buildings, including the excitation source and whether SSI effects were considered in the interpretation. For those building applications, we indicate the base fixity condition that the results apply for, where fixed- and flexible-base are as defined previously and pseudo-flexible base indicates that rotational SSI effects are included in the identified system flexibility, but not base translation (this is a common condition that occurs when input excitation is taken as base translation, per [2]).

Two families of methods are *parametric*, in the sense that system parameters are produced as the result of the identification process. One family of parametric system identification methods is referred to as *Realization Theory*. These approaches identify matrices describing first order differential equations relating input and output time series, known as a state-space realization. As shown in Table 2, alternative methods are distinguished by the input types that the methods can be used with, and by the statistical processes used to optimize the form of the matrix. Unlike the Prediction Error Methods described below, these methods do not minimize an error function. Realization Theory methods have been used to identify structural building properties (e.g., 4SID, ERA). When applied to structural problems, matrices computed from system identification are

related to properties describing the response of a multi-degree of freedom system with measured output and either assumed or measured properties of the input (impulse functions, white noise, earthquake-like time series). Commonly derived system properties are modal frequencies, damping ratios, and mode shapes. Most often the input is taken as the translational motion at the base of the structure and the output as the roof translation, which provides parameters descriptive of pseudo-flexible base conditions. One application of Realization Theory considers alternate input motions to provide modal properties for flexible- and fixed-base conditions [19-21] for structures with strong torsional coupling effects (e.g., irregular buildings). Reference-Based Stochastic Subspace Identification methods are output only, and as such provide flexible-base modal system parameters [11, 22].

The second family of parametric approaches is *Prediction Error Methods* (PEM), which seek to minimize error terms, defined as the difference between an observed output time series and the computed output time series given a parametric model with optimized coefficients. These approaches relate input to output time series in various ways. Modal minimization directly solves the equations of motion to produce the output series, repeating the process for a range of modal parameters, and seeking the combination of parameters that minimizes error between computed and measured output time series [23]. Another parametric approach relates input to output using polynomial expressions, where the order of the polynomials is double the number of modes. The expressions, in turn, can be related to modal properties (e.g. frequencies and damping ratios). PEM approaches have been used extensively to identify modal properties of structures for pseudo-flexible base conditions [1, 23, 25-28] in which the effects of SSI on parameters are not specifically evaluated, and for analysis of system response under alternate base fixity conditions to investigate SSI effects [2, 24, 30, 31]. Luco and de Barros [10] used parametric methods to evaluate fixed-base properties, which are needed to evaluate SSI effects.

In Table 2, the third family of system identification approaches is *non-parametric*. These procedures involve the interpretation of transfer functions of output/input motion pairs in the frequency domain without fitting an underlying model. In the Basic Frequency Domain technique, often known as “peak picking”, fundamental frequencies of the system are evaluated from the locations of local peaks in the transfer function, and damping is evaluated from the width of the peak (e.g., using half-power bandwidth method under the assumption of linearly viscous damping). This approach has been widely used, most often for earthquake excitation [e.g., 32, 33], but also for forced vibration [4, 7, 12,], and ambient vibration [11, 22]. Given the input/output signals that are generally selected, using the criteria developed in [2] and this study, the results from this work usually represent pseudo-flexible-base conditions for earthquake excitation and flexible-base conditions for forced vibration and ambient excitation. Enhanced Frequency Domain Decomposition and Random Decrement techniques are used for system identification with ambient loading [11, 22, 34, 35]. Blind Modal Identification methods are output only, and as such provide flexible-base modal system parameters [36, 37].

The last family consists of new methods that can be used to identify soil and structure attributes such as structural stiffness and mass matrices as well as soil impedance functions [37-39]. Bayesian methods of system identification have been applied for the identification of structural system parameters [40] with quantification of parameter uncertainty. Such approaches have not yet been applied for analysis of system response for different levels of base fixity.

Table 2. System Identification methods used in Earthquake and/or SSI applications

Family	Name and Reference	Input Type	Soln Domain	Application to Buildings [a]	System Properties Identified (base fixity: properties) [b]
Parametric: Realization Theory	Deterministic State-Space Real. [41]	Imp.	Time		
	Stochastic State-Space Real. [42]	Amb.	Time		
	Subspace State-Space Ident. (4SID) [43]	Any	Time	EQ, Amb: [39], ST: [34], Amb: [44]	~*: f, β, Φ [39]; [ ]: f, β, Φ [34]; unclear: f, β, Φ [44]
	Reference-Based Stochastic Subspace Identification [45]	Amb.	Time	Amb: [11, 22]	~: f [11, 22)]
	Eigensystem Real. Algorithm (ERA) [46]	Imp.	Time		
	Eigensystem Real. Algorithm (ERA) with Observer/Kalman Filter ID (OKID) [47]	Non-Amb.	Time	EQ: [48], ST: [34]	~: f, β [48]; [ ]: f, β [34]
	Eigensystem Real. Algorithm (ERA) with Multiple-reference Natural Excitation Technique (MNExT) [49]	Amb.	Time	ST: [34]	[ ]: f, β, Φ
	System Real. using Information Matrix (SRIM) [50]	Non-Amb.	Time	EQ: [19-21]	[ ], ~: f, β, Φ
	Extended Kalman Filter [51]	Non-Amb.	Time	EQ: [52]	[ ]: f, β
	General Real. Algorithm (GRA) [53]	Any	Time	ST: [34]	[ ]: f, β
Parametric: PEM	Maximum Likelihood Method [54]		Time		
	Least Squares Method [10]	Non-Amb	Freq.	FVS: [10]	[ ]: f, β, Φ
	Modal Minimization Method [23]	Non-Amb	Time	EQ: [23, 24]	~*: f, β [23]; [ ], ~*: f, β, Φ [24]
	AR or ARMA [18]	Amb.	Time		
	ARX, or ARMAX [18]	Non-Amb.	Time	EQ: [1, 2 25-31],	~*: f, β [1, 25-29]; [ ], ~*, ~: f, β [2, 30, 31]
Non-Parametric: Freq. Dom.	Basic Frequency Domain (BFD) technique, (AKA peak picking) [55]	Any	Freq	EQ: [32, 33], FVS: [7, 12], Amb: [11, 22] Amb, FVS: [4]	~*: f [32]; [ ]: f, β [33]; [ ], ~: f, β [10]; ~: f, β,Φ [4, 7]; ~: f [11, 22]
	Enhanced Frequency Domain Decomposition (FDD) [56]	Amb.	Freq	Amb: [33, 11, 22], ST: [34]	unclear: f, β, Φ [33]; [ ]: f, β, Φ [34]; ~: f [11, 22]
	Random Decrement (RD) Technique [35]	Amb.	Freq	Amb: [35]	[ ]: f, β, Φ
	Blind Modal Ident. [57, 58]	Non-Amb.	Freq-time	EQ: [36, 37, 57, 58]	~: f, β, Φ
New	Phy. model w. pre-set params [37-39]	Any	Time	EQ: [37, 38], EQ, Amb: [39]	K, M, soil springs
	Bayesian System Ident. [40]	Any	Time	EQ: [40]	K, M, C

[a] EQ = earthquake excitation, Amb = ambient noise excitation, ST = shake table experiments, FVS = forced vibration with shakers

[b] [ ], ~, ~* = fixed-, flexible-, and pseudo-flexible base, respectively. f, β, Φ = frequencies, damping ratios, mode shapes, respectively. K, M, C = structural stiffness, mass, and damping respectively.

Several methods in Table 2 could have been selected for the present analyses. As in [2], we selected parametric methods, primarily because they provide estimates of both frequency and damping for multiple base fixity conditions. Parametric methods that have been used previously for alternate base fixity conditions are ARX and SRIM. We select ARX. While the SRIM approach has been successfully applied for SSI problems, it was not selected because its additional complexity is most useful for irregular buildings with coupling of torsional and translational responses, which is not the case for the relatively simple model structures that comprise our intended application. We recognize that different system identification procedures could potentially be used to evaluate SSI effects; the input/output pairs presented subsequently may have useful applications with some of those approaches.

3.0 ASSESSMENT OF SUITABLE INPUT-OUTPUT SIGNAL PAIRS

We develop here the input/output motion pairs that can be used in parametric system identification to evaluate system properties at different levels of base fixity. This is accomplished by describing a model of a lumped mass structural system founded on a compliant base.

3.1 System Model

The system model in Figure 2(a) is a linear multi-degree of freedom structure with masses m_{si} and moments of inertia I_{si} (where i indicates superstructure degree of freedom) as well as foundation mass and moment of inertial m_f and I_f, respectively. Structural elements have stiffness and damping k_{si} and c_{si}. Soil compliance is modeled with springs that enable foundation translation (u_f) and rotation (θ_f) relative to free-field (undisturbed) ground. The overbar on spring stiffness in Figure 2 (e.g., $\bar{k}_x$ for translation) indicates a complex number, which introduces a phase shift between load demand and response that accounts for damping effects. Displacements of the structural masses relative to the translated and rotated foundation are denoted u_{si}.

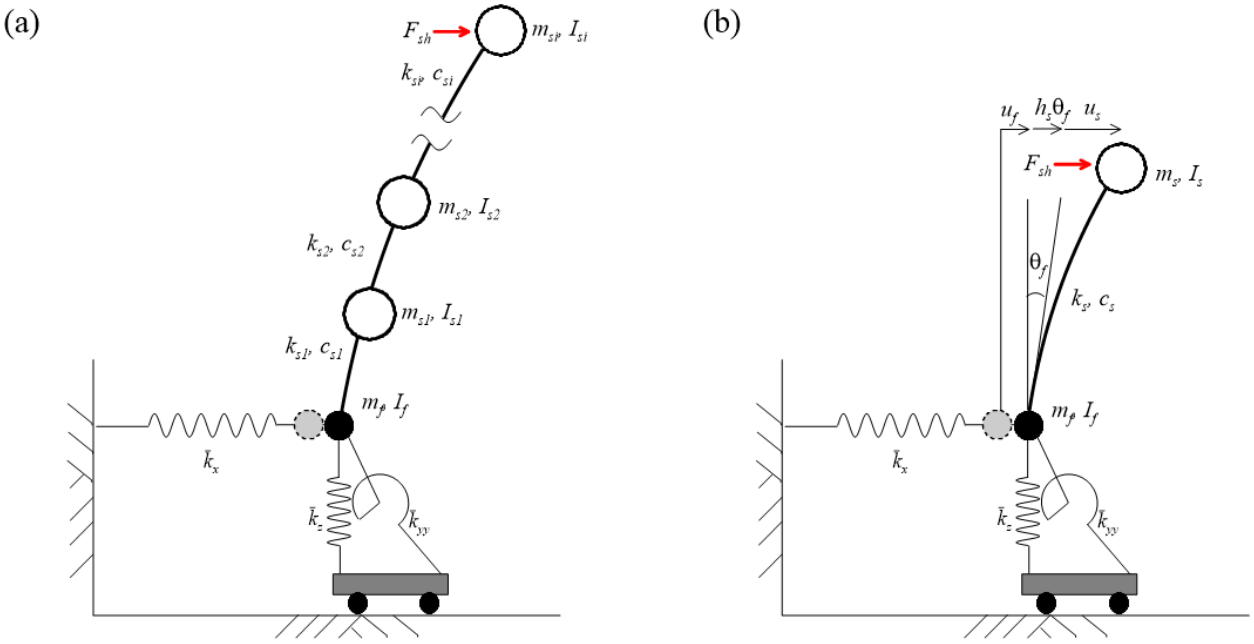

Figure 2. Simple SSI model subjected to forced vibration source

The equations of motion for the model in Figure 2a subjected to forced vibration is [59,60]:

$$\boldsymbol{M}\ddot{\underline{U}} + \boldsymbol{C}\dot{\underline{U}} + \boldsymbol{K}\underline{U} = \underline{F_{sh}} \tag{1}$$

where **M**, **C**, and **K** are the mass, damping and stiffness matrices (provided, for example in [55] for the case of three superstructure degrees of freedom). These matrices account for foundation degrees of freedom in translation (x) and rotation (yy) and each structural degree of freedom. Vectors $\underline{U}$ and $\underline{F_{sh}}$ are described further below.

Because our intended application is building models that can be characterized by a single superstructure degree of freedom (i.e., above the foundation mass), we proceed from this point using the simpler model in Figure 2(b). The solution for the more general case is similar to that presented here, and is given in Chapter 4 of [61]. For this case of a single degree-of-freedom superstructure subject to forced vibration, the terms in Eq. (1) can be written as:

$$\boldsymbol{M} = \begin{bmatrix} m_f + m_s & m_f h_f + m_s h_s & m_s \\ m_f h_f + m_s h_s & I_f + I_s + m_f h_f^2 + m_s {h_s}^2 & m_s h_s \\ m_s & m_s h_s & m_s \end{bmatrix} \tag{2a}$$

$$\boldsymbol{C} = \begin{bmatrix} c_x & c_{yx} & 0 \\ c_{xy} & c_{yy} & 0 \\ 0 & 0 & c_s \end{bmatrix} \tag{2b}$$

$$\boldsymbol{K} = \begin{bmatrix} k_x & k_{yx} & 0 \\ k_{xy} & k_{yy} & 0 \\ 0 & 0 & k_s \end{bmatrix} \tag{2c}$$

$$\underline{F_{sh}} = [F_{sh} \quad h_{sh}F_{sh} \quad F_{sh}\ ]^T \tag{2d}$$

$$\underline{U} = [u_f \quad \theta_f \quad u_s\ ]^T \tag{2e}$$

where h_f, h_s, and h_{sh} are the vertical distances from the bottom of the foundation slab to the center of mass of the foundation slab, the center of mass of the roof slab, and the center of mass of the shaker force, respectively (Figure 3). Terms k_x and k_{yy} are real-valued stiffness terms for the translational and rotational foundation degrees of freedom. Likewise, c_x and c_{yy} are dashpot coefficients. These parameters comprise the complex-valued impedance shown in Figure 2 [16]:

$$\bar{k}_j = k_j\left(1 + 2i\beta_j\right) \tag{3a}$$

where j is a subscript related to foundation degree of freedom (x or yy, respectively) and β_j indicates damping ratios defined as [16]:

$$\beta_j = \frac{\omega c_j}{2k_j} \text{ (defined for } k_j > 0) \tag{3b}$$

The off-diagonal soil impedance terms ($c_{yx} = c_{xy}$ and $k_{yx} = k_{xy}$) are coupling terms that describe the relationship between translational and rotational modes of vibration. The shaker force is F_{sh}. In

Eq. (1) the displacement vector $\underline{U}$ can be differentiated in time to corresponding velocity and acceleration vectors $\underline{\dot{U}}$ and $\underline{\ddot{U}}$, respectively.

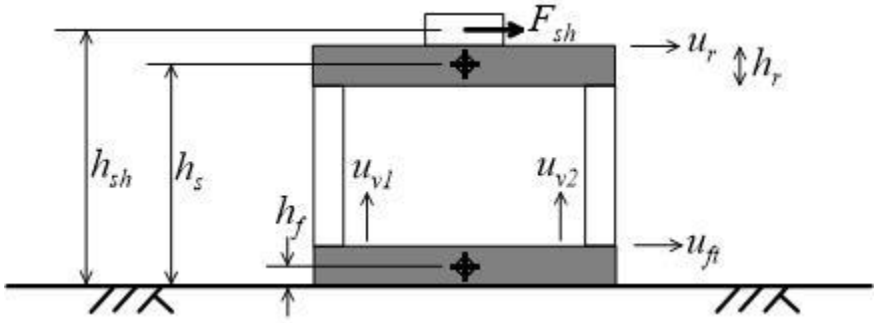

Figure 3. Schematic showing system dimensions and typical recorded quantities in forced vibration test

Following substitution of Eq (2) into Eq (1), it is possible to obtain algebraic equations for each degree of freedom. Excluding the $m_f h_f^2$ term, the $m_f h_f$ term, and the coupled foundation stiffness and damping terms, the equations are:

Foundation translation: $(m_s + m_f)\ddot{u}_f + m_s(h_s\ddot{\theta}_f + \ddot{u}_s) + c_x\dot{u}_f + k_x u_f = F_{sh}$ **(**4a)

Foundation rotation: $m_s h_s \ddot{u}_f + (m_s h_s^2 + I_f + I_s)\ddot{\theta}_f + m_s h_s \ddot{u}_s + c_{yy}\dot{\theta}_f + k_{yy}\theta_f = h_{sh}F_{sh}$ (4b)

Structural translation: $m_s(\ddot{u}_f + h_s\ddot{\theta}_f + \ddot{u}_s) + c_s\dot{u}_s + k_s u_s = F_{sh}$ (4c)

Following [2], for use with parametric system identification, it is convenient to convert Eq. (4) to the Laplace domain using the Laplace transform $g(t) = \hat{g}(s)e^{st}$, in which s is the Laplace variable. Recognizing that $\hat{\dot{u}} = s\hat{u}$, $\hat{\ddot{u}} = s^2\hat{u}$, and rearranging, Eq. (4) is re-written as:

$$(m_s + m_f)s^2\hat{u}_f + c_x s\hat{u}_f + k_x\hat{u}_f + m_s s^2(h_s\hat{\theta}_f + \hat{u}_s) = \hat{F}_{sh} \quad \textbf{(}5a)$$

$$(m_s h_s^2 + I_f + I_s)s^2\hat{\theta}_f + c_{yy}s\hat{\theta}_f + k_{yy}\hat{\theta}_f + m_s h_s s^2(\hat{u}_f + \hat{u}_s) = h_{sh}\hat{F}_{sh} \quad (5b)$$

$$m_s s^2\hat{u}_s + c_s s\hat{u}_s + k_s\hat{u}_s + m_s s^2(\hat{u}_f + h_s\ddot{\theta}_f) = \hat{F}_{sh} \quad (5c)$$

Following some rearrangement, we obtain:

$$(s^2 + 2\zeta_x\omega_x s + \omega_x^2)\hat{u}_f + \frac{m_s s^2(h_s\hat{\theta}_f + \hat{u}_s)}{(m_s + m_f)} = \frac{\hat{F}_{sh}}{(m_s + m_f)} \quad \textbf{(}6a)$$

$$(s^2 + 2\zeta_{yy}\omega_{yy}s + \omega_{yy}^2)\hat{\theta}_f + \frac{m_s h_s s^2(\hat{u}_f + \hat{u}_s)}{(m_s h_s^2 + I_f + I_s)} = \frac{h_{sh}\hat{F}_{sh}}{(m_s h_s^2 + I_f + I_s)} \quad (6b)$$

$$(s^2 + 2\zeta_s\omega_s s + \omega_s^2)\hat{u}_s + s^2(\hat{u}_f + h_s\hat{\theta}_f) = \frac{\hat{F}_{sh}}{m_s} \quad (6c)$$

where $\omega_s = \sqrt{k_s/m_s}$, $\omega_{yy} = \sqrt{k_{yy}/\left(m_s h_s^2 + I_f + I_s\right)}$, $\omega_x = \sqrt{k_x/\left(m_s + m_f\right)}$, $\zeta_s = c_s/(2\omega_s m_s)$, $\zeta_{yy} = c_{yy}/\left(2\omega_{yy}\left(m_s h_s^2 + I_f + I_s\right)\right)$, and $\zeta_x = c_x/\left(2\omega_x\left(m_s + m_f\right)\right)$.

Damping terms ζ_j are equivalent to β_j terms from classical solutions (as compiled in [16]) if moment of inertia terms are neglected and $m_f = 0$. The ζ_j notation accommodates these features.

Eq. (6) has three displacements and three equations, so each displacement can be solved for. Neglecting the moments of inertia and assuming, $m_s/(m_s+m_f) = 1$, and $h_s = h_{sh}$ the equations simplify to:

$$\hat{u}_f = \frac{\left(\frac{\hat{F}_{sh}}{m_s}\right)(B_{yy})(B_s)}{C} \quad \text{(7a)}$$

$$\hat{\theta}_f = \frac{\left(\frac{\hat{F}_{sh}}{m_s}\right)(B_x)(B_s)}{C h_s} \quad \text{(7b)}$$

$$\hat{u}_s = \frac{\left(\frac{\hat{F}_{sh}}{m_s}\right)(B_x)(B_{yy})}{C} \quad \text{(7c)}$$

In which $B_k = 2\zeta_k\omega_k s + \omega_k^2$ for $k = x$, yy, and s, and $C = B_x B_{yy} B_s + s^2\left(B_x B_s + B_x B_{yy} + B_{yy} B_s\right)$.

The derivation presented here is broadly similar to [2], which applied to earthquake excitation.

3.2 Evaluation of SSI Effects from Transfer Functions

Parametric system identification schemes [e.g, 1, 2] estimate transfer functions between input and output time series. For the present application, as in [2], the differences between these motions should represent the flexibility of system components related to the desired base fixity condition. In the Laplace domain, a transfer function can be defined as:

$$\hat{H}(s) \equiv \frac{Output}{Input} \quad (8)$$

Because Eq. 7 completely defines the displacements of the SSI system in the Laplace domain, transfer functions can be evaluated from those solutions for three relevant base fixity conditions:

(a) *Fixed-base.* For the fixed-base case, we take the input as the difference between the contribution of base slab translation and rocking to roof displacement and the shaker demand represented as acceleration ($\hat{F}_{sh}/m_s$). The output is the difference between the total roof acceleration and shaker demand. As a result, the difference between the input and output time series is only from structural flexibility, which is the desired result for fixed-based response. The transfer function is given by:

$$\hat{H}(s) = \frac{\hat{\ddot{u}}_f + h_s\hat{\ddot{\theta}}_f + \hat{\ddot{u}}_s - \frac{\hat{F}_{sh}}{m_s}}{\hat{\ddot{u}}_f + h_s\hat{\ddot{\theta}}_f - \hat{F}_{sh}/m_s} \quad (9)$$

If we substitute Eq. (7) into Eq. (9) the transfer function can be simplified to:

$$\widehat{H}(s) = \frac{B_x B_{yy} B_s}{C-(B_s B_x + B_s B_{yy})s^2} = \frac{(2\zeta_s \omega_s s + \omega_s^2)}{(s^2 + 2\zeta_s \omega_s s + \omega_s^2)} \tag{10}$$

The amplitude of $\widehat{H}(s)$ is a continuous surface with peaks (poles) for each mode that occur at a position on the horizontal plane which can be related to modal frequencies and damping ratios. The roots of the denominator of Eq. (10) are the poles (or peaks) of $\widehat{H}(s)$. The complex conjugate pairs are located as follows:

$$s_s, s_s^* = -\zeta_s \omega_s \pm i\omega_s \sqrt{1-\zeta_s^2} \tag{11}$$

from which the modal frequencies and damping ratios of the structure can be readily computed:

$$\omega_s = \sqrt{s_s s_s^*} \tag{12a}$$

$$\zeta_s = -\frac{Re(s_s)}{\omega_s} \tag{12b}$$

For undamped conditions, Eq. (11) represents the fundamental relation between the Fourier and Laplace variables $(s, s^* = \pm i\omega_s)$. System identification methods can be used to estimate the transfer function $\widehat{H}(s)$ from input and output signals as described below.

(b) *Pseudo-Flexible-base*. The pseudo-flexible base case accommodates base flexibility from rocking but not translation. This condition is important because, whether intentionally or not, it represents the level of base fixity for which many past studies have identified structural properties (Table 2). Accordingly, it is included here for completeness, even if this condition is not needed for typical SSI applications in which fixed- and flexible-base properties are the desired outcomes.

The input is the difference between base slab translational acceleration and shaker demand, while the output matches that for the fixed-base case. As such the difference between these two transfer functions is the inclusion within the identified system of base flexibility in rocking in the pseudo-flexible-base case. The transfer function is then:

$$\widehat{H}(s) = \frac{\hat{\ddot{u}}_f + h_s \hat{\ddot{\theta}}_f + \hat{\ddot{u}}_s - \frac{\hat{F}_{sh}}{m_s}}{\hat{\ddot{u}}_f - {\hat{F}_{sh}}/{m_s}} \tag{13}$$

$$\widehat{H}(s) = \frac{B_x B_{yy} B_s}{C - B_s B_{yy} s^2} = \frac{(2\zeta_{yy}\omega_{yy}s + \omega_{yy}^2)(2\zeta_s \omega_s s + \omega_s^2)}{(s^2 + 2\zeta_{yy}\omega_{yy}s + \omega_{yy}^2)(s^2 + 2\zeta_s \omega_s s + \omega_s^2) - s^4} \tag{14}$$

As before, the poles are values of *s* for which the denominator is zero. The roots have the same form as Eq. (11), but yield the following pseudo-flexible system modal frequency and damping ratio:

$$\bar{\omega}^2(s) = \frac{1}{\left({1}/{\omega_{yy}^2}\right) + \left({1}/{\omega_s^2}\right)} \tag{15a}$$

$$\bar{\zeta}(s) = \left(\bar{\omega}/\omega_{yy}\right)^3 \zeta_{yy} + \left(\bar{\omega}/\omega_s\right)^3 \zeta_s \tag{15b}$$

These pseudo-flexible-base expressions in Eq. (15) match the prior solution derived for earthquake loading [2] for the case of a foundation with zero mass and zero rotational inertia.

(c) *Flexible-base*. For the flexible-base case, the shaker demand comprises the input, while the output is as defined previously. As such, the system being analyzed includes all system displacement components in the difference between input and output. The transfer functions are:

$$\hat{H}(s) = \frac{\hat{\ddot{u}}_f + h_s\hat{\ddot{\theta}}_f + \hat{\ddot{u}}_s - \frac{\hat{F}_{sh}}{m_s}}{-\hat{F}_{sh}/m_s} \tag{16}$$

$$\hat{H}(s) = \frac{B_x B_{yy} B_s}{C} \tag{17}$$

The roots of the denominator are in the same form as Eq. (11) but with the system frequency $\tilde{\omega}$ and damping $\tilde{\zeta}$ defined as:

$$\tilde{\omega}^2(s) = \frac{1}{\left(1/\omega_x^2\right) + \left(1/\omega_{yy}^2\right) + \left(1/\omega_s^2\right)} \tag{18a}$$

$$\tilde{\zeta}(s) = \left(\tilde{\omega}/\omega_x\right)^3 \zeta_x + \left(\tilde{\omega}/\omega_{yy}\right)^3 \zeta_{yy} + \left(\tilde{\omega}/\omega_s\right)^3 \zeta_s \tag{18b}$$

Eq. (18) matches known theoretical solutions for flexible-base frequency and damping [2, 16, 62, 63], for the case of a foundation with zero mass and zero rotational inertia. The powers of 3 in Eq. (18b) correspond to the case of perfectly viscous damping. The alternative of a general frequency-dependent form and not perfectly viscous leads to powers of 2 [63].

To summarize, the input-output pairs to evaluate flexible-, pseudo-flexible- and fixed-base parameters for forced vibration testing are listed in Table 3. In Table 3, the format of motions matches the idealized locations shown in Figure 1, specifically u_f is displacement at the base of the foundation and u_s is structural deformation at the midpoint of the roof slab.

Figure 3 shows the minimal level of instrumentation that is required for the system identification described here. There are several differences from the idealized locations of motions depicted in Figure 1, namely (1) foundation translation is measured at the top of the foundation slab ($\ddot{u}_{ft}$), (2) rotation is not directly measured, but is evaluated from two vertical motions ($\ddot{u}_{v1}$ and $\ddot{u}_{v2}$), which assumes that the foundation is rigid in bending, and (3) roof translation is measured at the top of the roof slab ($\ddot{u}_r$). Top-of-foundation motion from a recording ($\ddot{u}_{ft}$) differs from the base-of-foundation motion used in the derivation ($\ddot{u}_f$) by an additional displacement from rotation $\ddot{\theta}_f$ over vertical distance $2h_f$. This is reflected in Footnote 1 (Table 3). A similar correction is required to adjust top-of-structure motion from a recording ($\ddot{u}_r$) to roof center of mass motion ($\ddot{u}_f + h_s\ddot{\theta}_f + \ddot{u}_s$) (Footnote 3). Footnote 2 shows the calculation of foundation rotation from two vertical motions.

Table 3. Input and output pairs to evaluate modal parameters for various base-fixity conditions. Response quantities are defined in Figure 1. Figure 3 shows measured quantities, and footnotes relate recorded time series to those used in system identification.

Base Fixity	Input[1,2]	Output[3]
Flexible-Base	$\frac{-F_{sh}}{m_s}$	$\frac{-F_{sh}}{m_s} + \ddot{u}_f + h_s\ddot{\theta}_f + \ddot{u}_s$
Pseudo Flexible-Base	$\frac{-F_{sh}}{m_s} + \ddot{u}_f$	$\frac{-F_{sh}}{m_s} + \ddot{u}_f + h_s\ddot{\theta}_f + \ddot{u}_s$
Fixed Base	$\frac{-F_{sh}}{m_s} + \ddot{u}_f + h_s\ddot{\theta}_f$	$\frac{-F_{sh}}{m_s} + \ddot{u}_f + h_s\ddot{\theta}_f + \ddot{u}_s$

1. $\ddot{u}_f = \ddot{u}_{ft} - 2\ddot{\theta}_f h_f$. Rotational acceleration computed from vertical sensors,
2. $\ddot{\theta}_f = (\ddot{u}_{v1} - \ddot{u}_{v2})/b$
3. $\ddot{u}_f + h_s\ddot{\theta}_f + \ddot{u}_s = \ddot{u}_r - (h_r/2)\ddot{\theta}_f$

4.0 VERIFICATION

4.1 Structural Model and Simulation Results

Here we verify the input-output pairs selected above by computing the elastic responses of a SDOF structure on a compliant soil medium (as depicted in Figure 2b) and utilizing those motions in parametric system identification analyses to see if the specified structural attributes are recovered. This example is also used to demonstrate steps in the system identification procedure.

The considered superstructure has structural stiffness k_s = 25974 kN/m, viscous damping ζ_s = 2%, element masses m_s = 13360 kg and m_f = 6980 kg, and zero element moment of inertia. The structure is square in plan with side dimensions of $2B$ = 3.0 m and H = 2.6 m. We consider two uniform, undamped soil conditions (Table 4). The frequency-dependent impedance is derived based on [62], as adapted for the present notation by [16].

Table 4. Properties of modeled linear soil-foundation-structural systems

Soil Profile	V_S **(m/s)**	ρ **(kg/m^3)**	f **(Hz)**	ζ_s **(%)**	$h/(V_sT)$	$\tilde{T}/T$	β_f **(%)**	$\tilde{f}$ **(Hz)**	β_0 **(%)**
Soft	107	1730	7.03	2.0	0.171	1.27	3.66	5.53	4.90
Stiff	213	1800	7.03	2.0	0.122	1.08	0.54	6.53	2.27

An eigenvalue analysis [55] of the modeled structure provides the undamped fixed-base frequency f. The resulting values of the wave parameter [16], which represents the ratio of structure to soil stiffness, are 0.171 and 0.122, which are large enough that significant inertial SSI effects are expected. Period lengthening ratio (ratio of flexible- to fixed-base periods) is computed with the following expression [62], with the results in Table 4:

$$\frac{\tilde{T}}{T} = \sqrt{1 + \frac{k_s}{k_x} + \frac{k_s h^2}{k_{yy}}} \tag{19}$$

Foundation damping (β_f) can be computed from expressions given in [16, 63]. The flexible-base damping (β_0) is then computed as:

$$\beta_0 = \beta_f + \frac{\zeta_s}{(\tilde{T}/T)^2} \tag{20}$$

We compute response using analytical solutions (modified from [59]) for forced vibration tests with excitation provided by a broadband, white noise, shaker excitation, F_{sh}. Figure 4 shows Fourier amplitude spectra of the shaker demand acceleration (top frame) and responses (bottom frame) for the case of the soft soil site. Although not shown in Figure 4, the responses have time lags relative to the demand reflective of system damping, which is an important aspect for the system identification to capture.

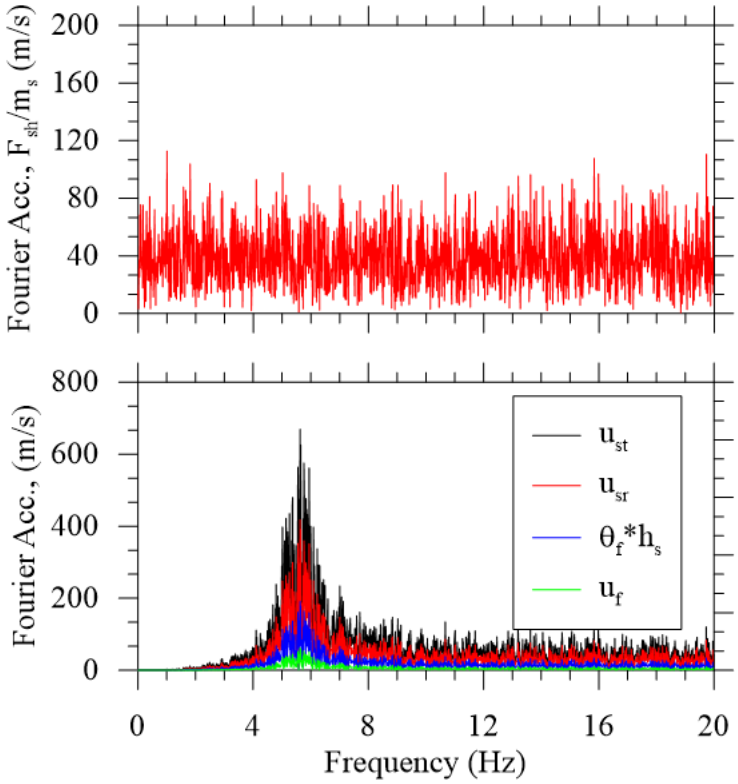

Figure 4. Modeled responses for the SDOF structures on soft soil with white noise shaker excitation

4.2 System Identification

Parametric system identification is applied using computed responses in the time domain. The shaker force and structure responses are manipulated to form the respective input and output pairs in Table 3. The manner by which a parametric ARX model is generated from an input/output time series is described elsewhere [65]; the key attributes that are user-selected are the time lag between

the input and output signals and the number of modes required to capture the system response. As described in [2], these parameters are selected iteratively by minimizing error between model output and observation, first for delay (using a fixed number of modes) and then for variable number of modes. The error is taken as:

$$V(\theta) = \sum_i \epsilon^2(t_i, \theta) \tag{21}$$

where $\epsilon(t_i, \theta)$ is the difference between model prediction and observation for time step t_i, θ is a set of model parameters describing the shape of the transfer function in the Laplace domain, and $V(\theta)$ is known as the Cumulative Prediction Error. Figure 5 shows the $V(\theta)$ vs lag and number of modes for the flexible-base identification of the structure on soft soil. For this input-output pair, the minimum error occurs at a time delay of zero and decreases gradually with an increasing number of modes. There are competing considerations regarding the selection of the number of modes – a low number is desired to avoid over-constraining the problem, but may introduce uncertainty due to sensitivity of modal damping (and sometimes frequencies) to the selected number of modes. We adopt the system identification steps from [65], which is briefly summarized as follows:

- Assume one mode and evaluate lag
- Using this lag, perform system identification initially with a small number of modes (typically two), and incrementally increases the number until modal results have stabilized.
- Check that the original lag is appropriate with the selected number of modes, and adjust as needed.
- Check the suitability of the solution by examining the model fit to data in the frequency domain (transfer function) and time domain (measured and estimated output time series). Also check that zeros and poles in the transfer function are inside the unit circle and that the input and output residual are uncorrelated with high confidence.

For the present problem, we select a lag of zero and four modes.

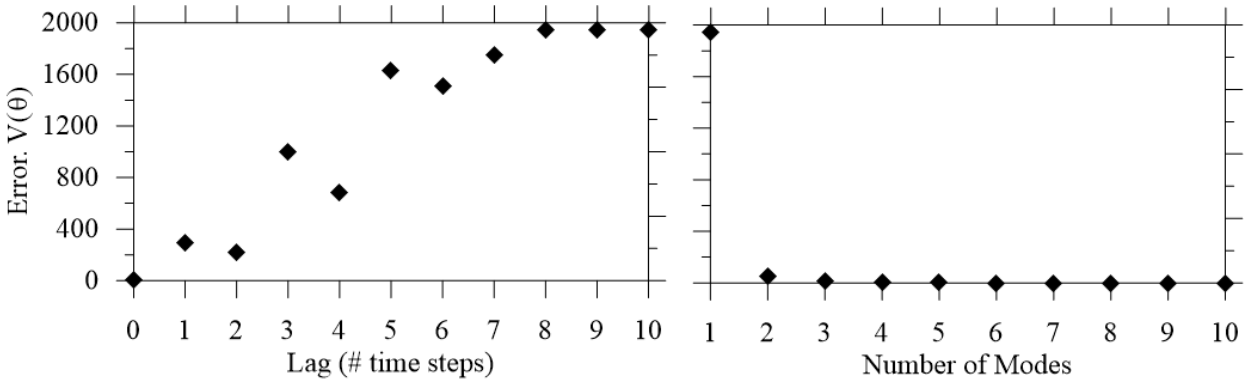

Figure 5. Error of system identification model with respect to (a) time delay for 1 mode and (b) number of modes for zero lag

The transfer function surface in the Laplace domain is computed for the selected lag and number of modes. Examples of these surfaces using data from test structures is provided in the next section. Peaks (or poles) in the transfer functions are related to modal frequencies and damping ratios per Eq. (12), with the results given in Table 5. Matches are good for both frequencies and damping. Based on these findings, we conclude that the use of the input-output pairs shown in Table 3 in system identification analysis provides accurate estimates of modal parameters.

Table 5. Summary of specified and back calculated fixed-base and flexible-base frequency and damping results

Soil Profile	Fixed-Base Parameters				Pseudo-Flexible-Base Parameters				Flexible-Base Parameters			
	Specified		System ID		Specified		System ID		Specified		System ID	
	f (Hz)	ζ (%)	f (Hz)	ζ (%)	$\tilde{f}^*$ (Hz)	$\tilde{\zeta}^*$ (%)	$\tilde{f}^*$ (Hz)	$\tilde{\zeta}^*$ (%)	$\tilde{f}$ (Hz)	$\tilde{\zeta}$ (%)	$\tilde{f}$ (Hz)	$\tilde{\zeta}$ (%)
Soft	7.03	2.00	7.03	2.00	5.81	3.83	5.82	3.82	5.53	4.90	5.55	4.92
Stiff	7.03	2.00	7.03	2.00	6.65	1.97	6.64	1.97	6.53	2.27	6.53	2.27

5.0 APPLICATION

5.1 Field Testing of Test Structures

Figure 6 shows two model structures constructed for forced-vibration testing of shallow foundations experiencing combined base shear and moment demands. The smaller test structure (right side in Figure 6) is portable and has been used at two sites (Garner Valley Downhole Array [GVDA] and the Wildlife Liquefaction Array [WLA]) with separate cast-in-place shallow foundations. The larger structure (left side in Figure 6) is permanently installed at the GVDA site. Both structures have reinforced concrete foundations and upper slabs and intermediate steel columns (details in [15] and [14], respectively). The structures were designed with removable steel square tube cross-bracing to facilitate modification of structural stiffness. The portable structure is rectangular in plan, whereas the permanent structure is square. Structural and ground responses are monitored through an array of accelerometers. In addition, vertical displacement sensors and pressure sensors were installed at or across the soil-foundation interface. Careful attention was paid to synchronization of the measurements of shaker forces and structural responses so that delays between forces and responses arise from structural responses and not relative instrument delays, as discussed further in [15]. These considerations are important for estimates of damping.

Figure 6. Two SFSI structures, the portable test structure (right) and the permanent structure (left) located at GVDA

General attributes of these structures are summarized in Table 6 following the notation in Figure 3 for dimensions and Figure 2(b) for masses. Plan view dimensions of the foundation (and roof slabs) are 2*B* (short direction) and 2*L* (long direction). Frequencies and damping ratios in Table 6 for the portable structure were determined by examining free-decay of the structure when affixed to a strong floor in the UCLA structural engineering laboratory. As such, these can be considered as low-amplitude fixed-base frequencies. Laboratory vibration measurements of this sort were not performed for the permanent test structure.

Table 6. Attributes of test structure. Modal properties are from fixed-based testing in UCLA structures lab

Struc.	**Site**	h_s **(m)**	h_r **(m)**	$2h_f$ **(m)**	$2B$ **(m)**	$2L$ **(m)**	m_s **(kg)**	m_f **(kg)**	f **(Hz)**[1]	ζ[1]
Port.	GVDA, WLA	2.88	0.25	0.61	2.14	4.28	6980	13340	32.5 (Xb)	0.014 (Xb)
									21.4 (Yb)	0.024 (Yb)
									11.8 (Xu)	0.013 (Xu)
									11.6 (Yu)	0.013 (Yu)
Perm.	GVDA	4.56	0.40	0.50	4.06	4.06	16400	20500	-	-
									-	-

[1] X, Y: Loading directions, where X is longitudinal and Y is transverse; b=braced, u=unbraced

The GVDA site has medium dense sedimentary deposits, while the WLA site has soft clays overlying loose liquefiable soils. Figure 7 shows available shear wave velocity (V_S) profile data (compiled by [15]), along with representative profiles considered for the present work. In developing the profiles selected for analysis we gave preference to suspension logging methods at depth, which have higher resolution than the alternative profiles based on surface wave measurements. Following recommendations in NIST [16], representative values of V_S are taken as time-averaged velocities over profile depths (z_p), which in turn are related to the foundation

moment of inertia applicable to the direction of shaking. Table 7 lists applicable z_p values and the time-averaged small-strain shear wave velocities ($V_{s,avg}$) computed for those depth intervals.

Both test structures have recorded dynamic responses from several excitation sources. Small earthquakes were recorded on the permanent structure at GVDA and on the portable structure while it was at WLA. Forced vibration loading from a small linear mass electromagnetic shaker was applied in both directions to the portable structure and in one direction for the permanent structure. The linear mass shaker imposes low-amplitude loads on the structures and soil behavior is expected to remain nearly linear visco-elastic. Forced vibration loading was also applied with an eccentric mass shaker to the portable test structure in both directions. This shaker applies larger demands that can develop non-linear soil behavior.

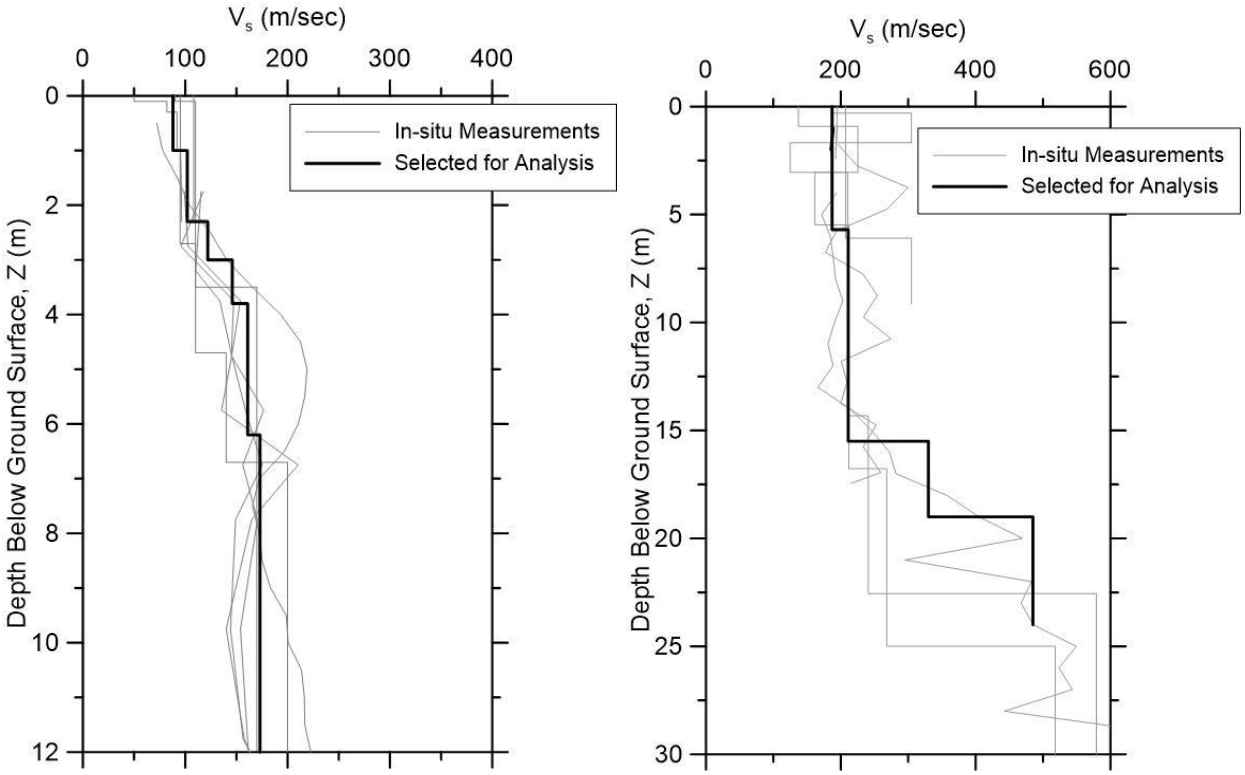

Figure 7. Measured shear wave velocity data for WLA site (left) and GVDA site (right) along with profiles used for analysis in this paper.

Table 7. Structure- and direction-specific depth-averaged small-strain shear wave velocities for SSI analysis

Structure	**Sites Tested**	**Loading Dir.**	**z_p (m)**	**$V_{s,avg}$ (m/s)**
Portable	WLA	X	3.59	106
		Y	2.54	97
	GVDA	X	3.59	187
		Y	2.54	187
Permanent	GVDA	X=Y	4.06	187

Table 8 summarizes conditions for which vibration responses have been recorded for the test structures, both from forced-vibration tests and earthquakes. The wave parameter $h_s/(V_{s,avg}T)$ indicates the expected significance of inertial SSI for each set of experiments [16], and is shown for small-strain conditions. For the case of the portable structure, fixed base properties used in the wave parameter calculation are from Table 6 (laboratory measurements on strong floor). For the permanent structure, we use fixed-base properties from system identification in the next section (12.8 Hz with bracing, 6.7 Hz without bracing). The range of wave parameter values, $0.15 - 1.31$, is large relative to the approximate range previously encountered for buildings under earthquake excitation of $0 - 0.4$ [66]. In Table 8 we do not show wave parameter values for tests where nonlinear effects are expected (i.e., EMS and Eqk sources), although such effects are considered subsequently.

Table 8. Attributes of forced vibration experiments and earthquake recordings at instrumented field test structures

Structure [Ref]	Site	Bracing	Load. Source[1]	Load. Dir.[2]	X: $h_s/(V_{S,avg}T)$	Y: $h_s/(V_{S,avg}T)$
Portable [15]	WLA	Braced	EMS	X, Y		
			LMS	X, Y	0.95	1.31
		Unbraced	EMS	X, Y		
			LMS	X, Y	0.30	0.30
			Eqk	X, Y		
	GVDA	Braced	EMS	X, Y		
			LMS	X, Y	0.54	0.68
		Unbraced	EMS	X, Y		
			LMS	X, Y	0.17	0.15
Permanent [14]	GVDA	Braced	LMS	X=Y	0.31	0.31
		Unbraced	LMS	X=Y	0.16	0.16
			Eqk	X=Y		

[1] EMS = eccentric mass shaker; LMS = linear mass shaker; Eqk. = earthquake

[2] X = shaking in longitudinal direction; Y = shaking in transverse direction

5.2 System Identification to Evaluate Soil-Structure Interaction Effects

Here we apply parametric system identification procedures using data from the field test structures to identify fixed- and flexible-base properties. Parametric system identification is performed using the input/output signals developed above for forced vibration tests and in [2] for earthquake data; a few exceptions involving forced vibration testing where parametric procedures are not used are described below. The data sets considered in this study are archived and publicly available [15].

The optimal lag time and number of modes for each input-output data set are obtained in the same manner described in Section 4. Since there can be changes of modal parameters as the number of modes is adjusted, for a given test, we use a consistent number of modes for each base fixity condition so that differences between results are more likely to represent the SSI effect and less likely to be artifacts of the system identification process. Figure 8 shows example transfer function

surfaces for the fixed- and flexible-base cases for the portable structure at WLA with and without bracing, shaken in the X-direction. The locations of the poles define modal frequencies and damping ratios per Eq. (12a) and (12b). As shown in Figure 8, the braced structure has two significant modes - the lower frequency response in the flexible base plot (near 10.5 Hz) comprises the system response of interest. The higher frequency response in the fixed base plot (near 16 Hz) is associated with bracing vibrations. The overall fixed base response occurs near 35 Hz.

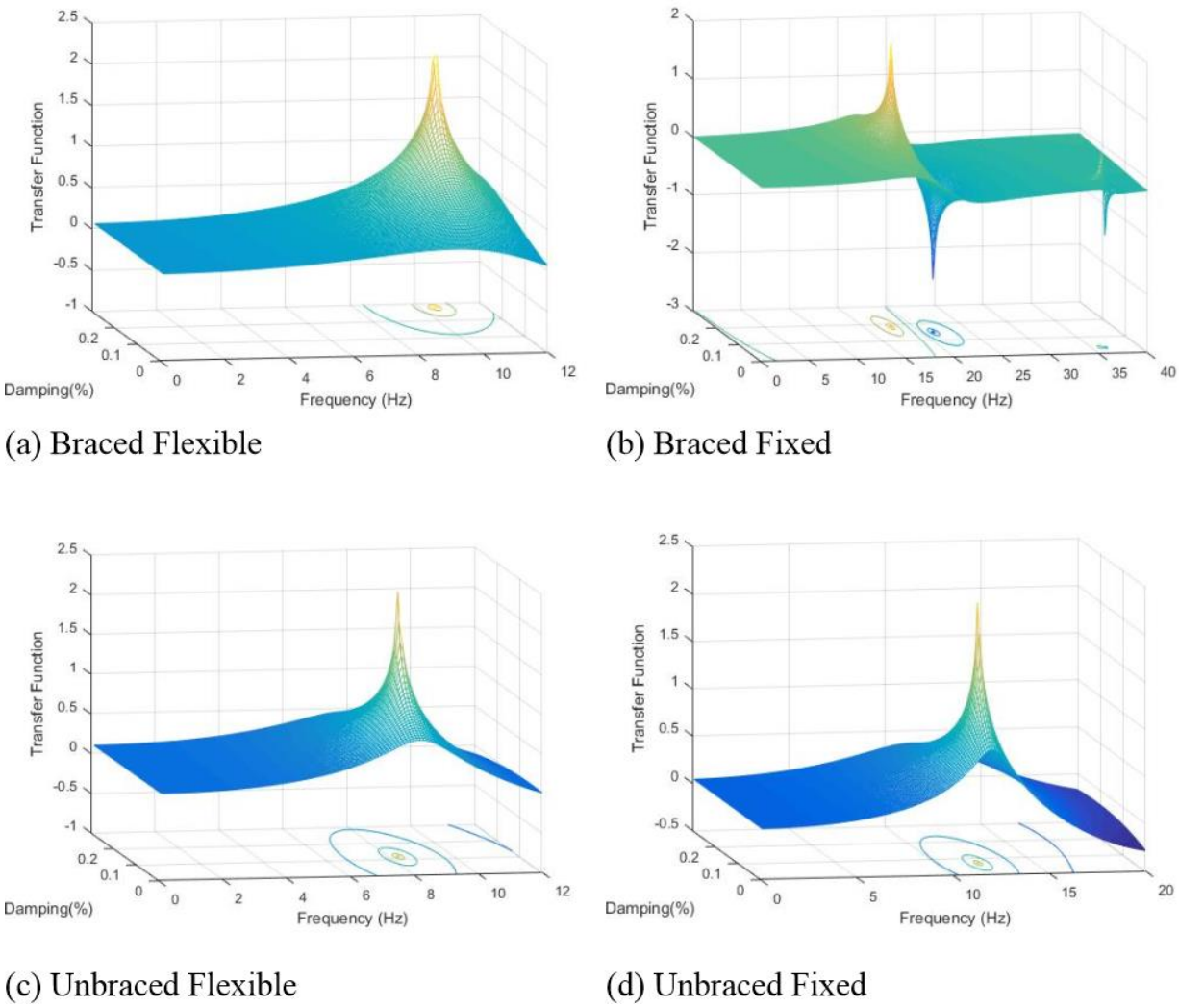

Figure 8. Transfer function surfaces showing locations of poles for portable structure at WLA site subject to forced vibration testing using LMS in X-direction.

As in [2, 65], we performed several checks of the parametric system identification results for each input/output data pair, including (1) plotting output time series from the identified model and data, to check compatibility and (2) plotting the intersection of the transfer function with a vertical plane

on the frequency axis with a non-parametric transfer function. Results of these checks are given in [61, 67, 68] and while not shown here for brevity, they confirm the identified modal parameters.

Because the data from test structures involves excitations at variable levels of demand that can produce soil responses that extend into the nonlinear range, we estimate approximate strain demands for each test. We compute an index that approximates shear strain (γ_{eff}^{I}) near the foundation-soil contact based on the foundation peak velocity (*PGV*) and soil shear wave velocity near the ground surface (V_{S0}) as (modified from [69]):

$$\gamma_{eff}^{I} = n\frac{PGV}{V_{S0}} \tag{22}$$

where *n* is taken as 1.0 for cyclic forced vibration tests and as (**M**-1)/10 for earthquake loading [70], and *PGV* is computed for each test by integrating the average recorded horizontal acceleration response of the foundation. For the value of γ_{eff}^{I} for each test, we estimate the soil shear modulus reduction (G/G_0) and damping (β_s) using generic models by Menq [71] for sand and Darendeli [72] for fine-grained soils.

The system identification procedures described above were repeated for all forced vibration test data sets. Results are shown in Table 9 along with estimated shear strains, γ_{eff}^{I}. Note that frequency ratio $f/\tilde{f}$ is equivalent to period lengthening. Notable attributes of the results include: (1) stronger SSI effects (i.e., larger period lengthening and foundation damping) for the braced vs unbraced configurations; (2) generally stronger SSI when strains are large enough to induce nonlinear soil response (although in some cases damping does not increase with strain level); and (3) lack of a consistent trend in SSI effects for shaking in the short vs long directions of the structure. The trends observed are generally compatible with expectation in the sense that factors that increase observed inertial SSI effects also increase $h_s/(V_{s,avg}T)$.

For a few cases (most notably the braced structure with shaking in the Y direction) the system identification for the fixed-base condition produced unstable estimates of modal parameters with respect to the selected value of *J* (number of modes). These attributes were considered to be unreliable, for the reason that the identified properties were generally poorly matched to results of testing in the UCLA structures lab (Table 6), and are not shown in Table 9. The unreliable results in this case are likely due to the small amplitude of the structural displacements for the braced structure. Accordingly, for subsequent analysis in this paper, the fixed-base frequencies for such cases are taken from Table 6 and the fixed-base damping is taken as the approximate average value from Table 6 of 1.5%. Fixed-based conditions where these properties are applied are marked with '-' in Table 9. In all other cases, fixed-base properties are identified from system identification procedures. There are small differences in fixed-base properties of the portable structure between excitation sources and between sites, despite the same structure having been used in each test. This occurs because of unavoidable variations in the rigidity of bolted connections. For example, the LMS source produces frequencies of 11.7 and 11.2 Hz for X direction responses of the unbraced structure at the two sites. Likewise, the stronger excitation from the EMS source produces fixed-base frequencies of 9.7 and 10.7 Hz for the same conditions. These variations in the condition of the structure do not affect the reliability of period lengthening and foundation damping from the tests, which are evaluated on a case-by-case basis for individual tests.

For the case of earthquake loading of the portable structure at the WLA site, system identification of flexible-base parameters was not possible due to a lack of appropriate free-field acceleration records. While the WLA site is instrumented with ground accelerometers, the closest instrument was approximately 70 m from the test structure. Accordingly, flexible-base properties were estimated from pseudo-flexible and fixed-base properties using procedures described in [2].

Table 9. System identification of instrumented field test structures

Struc.	Site	Bracing	Load. Source[1]	Load. Dir.[2]	System ID Results							γ_{eff}^{I}
					f (Hz)	ζ (%)	$\tilde{f}^{*}$(Hz)	$\tilde{\zeta}^{*}$ (%)	$\tilde{f}$ (Hz)	$\tilde{\zeta}$(%)	$f/\tilde{f}$	
Portable	WLA	Braced	EMS	X	31.9	2.54%	10.3	11.15%	9.7	13.52%	3.31	0.00252
				Y	-	-	8.0	18.73%	6.9	18.10%	3.21	0.00312
			LMS	X	35.7	3.51%	12.5	14.20%	11.2	28.95%	2.87	0.00029
				Y	-	-	9.6	18.07%	8.1	24.94%	2.70	0.00046
		Unbraced	EMS	X	9.7	-	8.6	8.10%	8.1	8.53%	1.48	0.00251
				Y	9.1	-	7.1	8.70%	6.6	8.89%	1.38	0.00235
			LMS	X	11.7	4.43%	9.1	5.01%	8.5	7.48%	1.38	0.00035
				Y	10.1	-	7.4	6.31%	7.0	7.26%	1.44	0.00049
			Eqk. M=4.8	X	12.1	1.08%	9.1	4.24%	8.5[3]	7.05%[3]	1.33	0.00300
				Y	12.2	1.73%	7.4	3.05%	7.2[3]	7.27%[3]	1.65	0.00660
	GVDA	Braced	EMS	X	-	-	13.1	10.79%	12.0	11.03%	2.68	0.00208
				Y	23.3	7.67%	9.8	10.90%	8.8	12.32%	2.51	0.00198
			LMS	X	36.9	1.52%	14.9	7.48%	14.2	9.41%	2.25	0.00010
				Y	-	-	11.7	6.43%	10.9	8.14%	2.02	0.00018
		Unbraced	EMS	X	10.7	-	9.5	5.57%	9.0	5.12%	1.33	0.00241
				Y	11.6	7.42%	8.0	5.13%	7.6	5.03%	1.52	0.00187
			LMS	X	11.0	1.27%	10.2	2.12%	9.8	3.13%	1.12	0.00021
				Y	11.2	1.32%	9.1	2.33%	8.8	3.06%	1.27	0.00021
Permanent	GVDA	Unbraced	LMS	-	7.1	0.32%	6.0	1.53%	5.9	2.00%	1.21	0.00013
			Eqk. M=4.2	-	6.7	0.51%	-	-	5.8	1.25%	1.15	0.00170
			Eqk. M=5.4	-	6.7	0.90%	-	-	5.8	4.11%	1.15	0.00170

[1] EMS = eccentric mass shaker; LMS = linear mass shaker; Eqk. = earthquake

[2] X = shaking in longitudinal direction; Y = shaking in transverse direction

[3] Flexible-base properties were estimates from pseudo-flexible and fixed-base properties using procedures described in [2]

5.3 Comparison of Experimental Results to Model Predictions

We compare the experimental results to predictions from models for period lengthening and foundation damping. For period lengthening, we follow the classical approach of Veletsos and Meek [62] (Eq. 19) as implemented in [16], which includes recommendations for adapting impedance expressions for non-uniform profiles. For foundation damping (β_f in Eq. 20), we use expressions in [16, 63]. These models represent the state of practice due to their incorporation, with minor modification, into the ASCE 7/16 standard [17]. The only modification to these models applied for this application was to adjust soil properties in an equivalent linear sense. We compute the shear strain using Eq. (22) and then strain-adjust the shear modulus (G) and soil hysteretic damping (β_s) used in the period lengthening and foundation damping expressions (using models for nonlinear soil response by [71, 72]).

The input parameters used for these calculations are given in Table 6 for structural parameters and Table 7 for small-strain soil parameters. Figure 9 shows values of period lengthening $\tilde{T}/T$ and foundation damping β_f plotted against wave parameter $h_s/(V_{s,avg,\gamma}T)$, where $V_{s,avg,\gamma}$ is the average shear wave velocity adjusted for nonlinear effects. Also shown in Figure 9 are model predictions for the range of aspect ratio (h_s/B) present in the specimens, which is 2.0-2.7.

As shown in Figure 9, the softer WLA site (black symbols) experiences larger SSI effects (i.e., increased period lengthening and foundation damping) than the stiffer GVDA site (red symbols). However, there is data overlap, and there are no particular differences between results for the two sites in the overlap region.

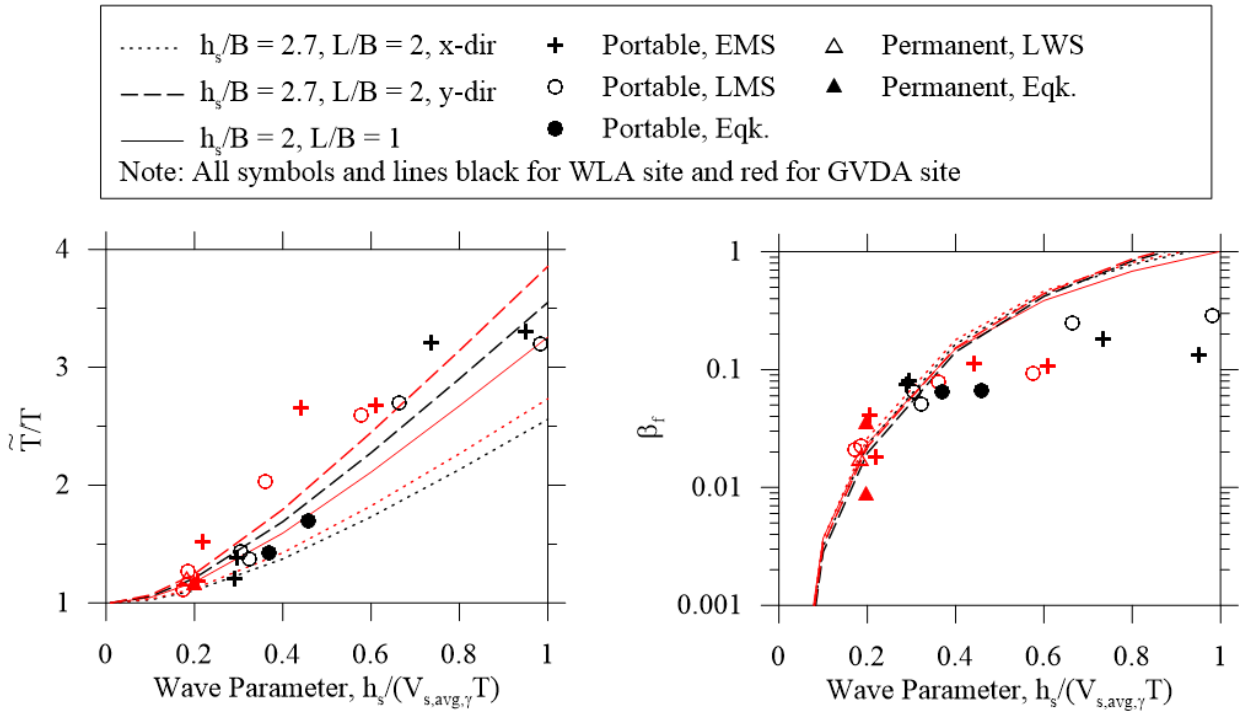

Figure 9. Period lengthening and foundation damping versus wave parameter for predictive models (lines) and based on system identification using recorded motions of test structures (discrete symbols) for various loading sources. In the figure, black and red solid lines (for $h_s/B = 2$) overlap.

The model predictions shown in Figure 9 assume full contact area between foundation and soil, which is violated when gaps form. For relatively weak shaking as provided by the EMS, we anticipate that there should be nearly full contact, as evidence of gapping was not observed in the field. Gap formation was observed during LMS shaking. Figure 10 illustrates the sensitivity of model predictions to contact area by showing sets of model predictions for full foundation contact and for a 50% reduction in contact area. The area reduction is applied to the horizontal foundation dimension in the direction of shaking. Log scales are used in Figure 10 to better visualize trends for small values of period lengthening and foundation damping. Reducing foundation contact area increases predicted period lengthening and decreases foundation damping. The 50% contact area reduction, while admittedly somewhat arbitrary, improves the fit in several cases. Our intent in showing these results is to illustrate how gapping may have contributed to the observed responses at higher load levels. We have not sought to optimize fits by systematically varying the contact area for each test. However, in general full contact area provides the best match to EMS results and 50% reduction provides improved match for LMS results.

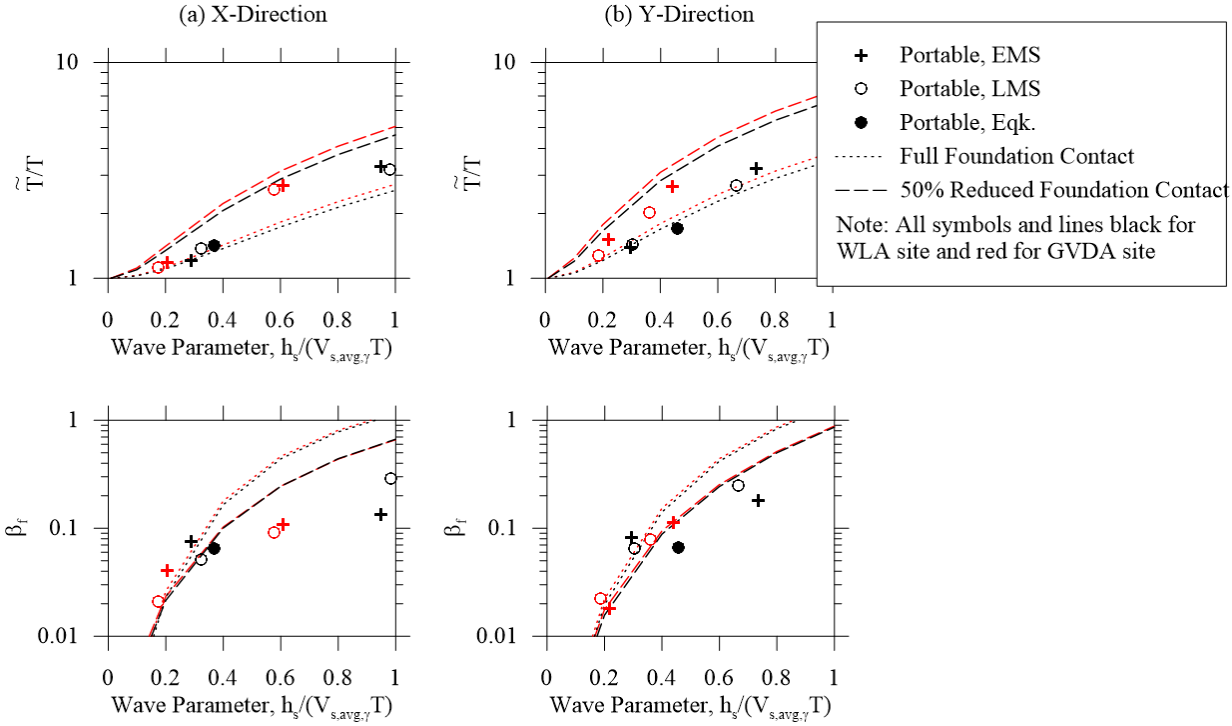

Figure 10. Period lengthening and foundation damping versus wave parameter for various loading sources on the portable structure at the WLA site (black) and GVDA site (red) for a) X-direction and b) Y-direction excitation.

Model performance can be more directly assessed using residuals, defined as follows:

$$R^T = \frac{\left(\frac{\tilde{T}}{T}\right)_{obs} - \left(\frac{\tilde{T}}{T}\right)_m}{\left(\frac{\tilde{T}}{T}\right)_m} \tag{23}$$

$$R^D = \frac{(\beta_f)_{obs} - (\beta_f)_m}{(\beta_f)_m} \tag{24}$$

where subscript '*obs*' indicates observation (from Table 9) and subscript '*m*' indicates model prediction. Model predictions are based on full contact area. Residuals are plotted against wave parameter $h_s/(V_{s,avg,\gamma}T)$ and strain index γ^I_{eff} in Figure 11. Residuals for period lengthening are generally positive and increase with wave parameter. Residuals for the GVDA site are generally larger than for the WLA site for the same wave parameter. Residuals do not appear to trend with strain index, indicating that nonlinearity has been reasonably captured by the models. Residuals from damping are generally positive at small wave numbers and increasingly negative at large wave numbers. As with period lengthening, the damping residuals do not trend with strain index. Some of the bias in Figure 11 likely results from reduced foundation-soil contact area from gapping, particularly for results derived from the EMS source. We have not attempted to empirically adjust our analysis procedures to remove bias, which in principle could be done with further changes to the contact area and the nonlinear adjustment of soil properties.

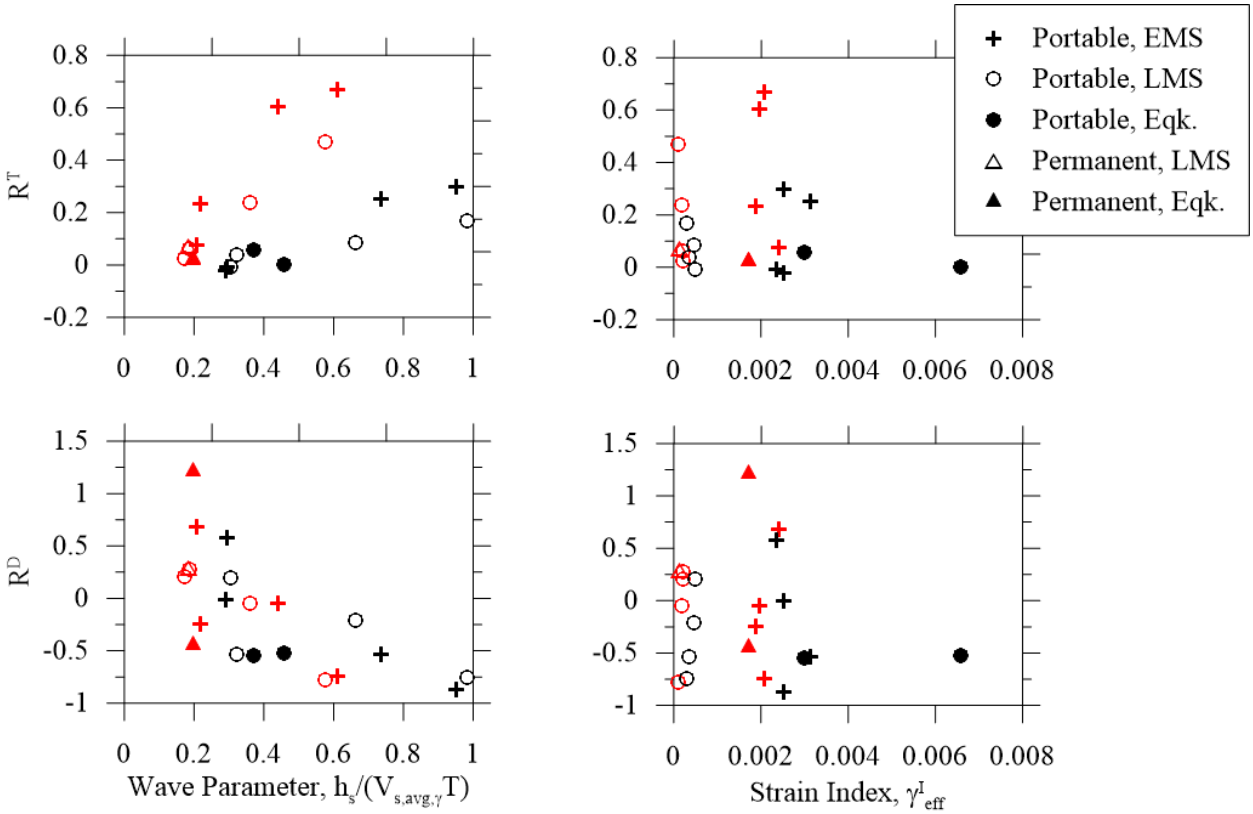

Figure 11. Residuals of system identification compared to predictive models for period lengthening (top row) and foundation damping (bottom row) versus wave number and strain index. Red symbols GVDA, black symbols WLA.

6.0 CONCLUSIONS

Parametric system identification of data recorded during forced vibration tests provides a useful tool for evaluating modal frequencies and damping ratios, which in turn can be interpreted to evaluate soil-structure interaction effects for tested structures. In this study, we have extended parametric system identification procedures developed for earthquake excitation to the case of forced vibration. To evaluate flexible-base modal parameters, which incorporate flexibility and

damping associated with foundation translation and rocking along with structural translation, recordings of shaker force and roof translational acceleration are needed. Also required are masses of the shaker and structure and structural dimensions. All relevant masses, including shaker mass associated with the term (F_{sh}/m_s) should be known with accuracy to allow a reliable estimation of modal parameters at high frequencies. This is in contrast to earthquake loading, where the input and output terms do not depend on mass. To evaluate pseudo-flexible-base parameters (in which foundation translation is not considered as a source of system flexibility), the input to the system identification incorporates the foundation translation, such that the difference between input and output does not include this effect. Similarly, for fixed-base modal parameters, both foundation translation and base rocking are required, such that the difference between output and input is only the structural deformation. Recommended input-output pairs for each case are given in Table 3.

The input-output pairs listed in Table 3 have been verified using simulations of simple structure-foundation-soil systems. The properties of the systems were specified, simulations were performed that produced time series of responses, and those time series were adapted for use in system identification. Results of this exercise were favorable with regard to both first mode frequencies and damping ratios for difference base fixity conditions, thus verifying the recommended input/output pairs.

The recommended system identification procedures were applied to recordings obtained during forced vibration testing and earthquake shaking of two test structures. One of the structures is portable and has been used for testing at two sites. The other structure is permanently installed at the Garner Valley site. System identification results are interpreted in the form of period lengthening ratios and foundation damping. Some of the unique aspects of this data set are that (1) the results apply for a range of shaking demands spanning from visco-elastic to nonlinear soil responses, and (2) the results apply for a broad range of the wave parameter. We find a strong association of wave parameter with both period lengthening and foundation damping, even among multiple tests on the same structure.

We suggest an approximate means by which to account for soil nonlinearity in model predictions using an equivalent-linear approach. We find that models recently presented by NIST [16] for period lengthening and foundation damping generally provide reasonable first order predictions of these effects, including the effect of nonlinearity, although the model predictions could be improved in future work through consideration of gapping at the foundation-soil interface.

7.0 ACKNOWLEDGEMENTS

Support for this work was provided by the National Science Foundation (NSF). This work was completed as part of a multi-institutional NSF grand challenge (NSF 06-504 Program) project, “Mitigation of Collapse Risk in Vulnerable Concrete Buildings” documented at the DesignSafe-CI website, https://www.designsafe-ci.org, as project NEES-2008-0637. Support of NEES@UCSB and NEES@UCLA was provided by the George E. Brown, Jr. Network for Earthquake Engineering Simulation (NEES) Program of the National Science Foundation (NSF) under Award Number CMMI-0927178.

This research made broad use of the field equipment, instrumentation, and technical expertise of the NEES@UCLA research group, including Dr. Robert Nigbor, Steve Keowen, Steve Kang, Dr.

Alberto Salamanca, and Ben Ferraro. Several NEES@UCSB sites were used during this research and Dr. Jamison Steidl, and his team, assisted during set up and testing. The NEES@UCSB also provided additional data from the permanent structure. The NEES@UTexas team provided the use of their field equipment and for performing additional geophysical testing at the field sites. We are grateful for the input on this paper provided by three anonymous reviewers and the responsible editor.

8.0 REFERENCES

1. Şafak E. Identification of linear structures using discrete–time filters. *J of Structural Engineering* 1991; 117: 3064-3085.
2. Stewart JP, Fenves GL. System identification for evaluating soil-structure interaction effects in buildings from strong motion recordings. *Earthquake Engineering & Structural Dynamics* 1998; 16: 1-21.
3. De Sortis A, Antonacci E, Vestroni F. Dynamic identification of a masonry building using forced vibration tests. *Engineering Structures* 2005; 27 (2): 155-165.
4. Trifunac MD. Comparisons between ambient and forced vibration experiments. *Earthquake Engineering & Structural Dynamics* 1972; 1 (2): 133-150.
5. Farrar CR, James GH. System identification from ambient vibration measurements on a bridge. *J of Sound and Vibration* 1997; 205 (1): 1-18.
6. Satake N, Suda K, Arakawa T, Sasaki A, Tamura Y. Damping evaluation using full-scale data of buildings in Japan. *J of Structural Engineering* 2003; 129 (4): 470-477.
7. Bradford SC, Clinton JF, Favela J, Heaton TH. Results of Millikan Library forced vibration testing. Technical report 2004, California Institute of Technology, http://resolver.caltech.edu/CaltechEERL:EERL-2004-03.
8. Wong HL, Trifunac MD, Luco JE. A comparison of soil-structure interaction calculations with results of full-scale forced vibration tests. *Soil Dynamics & Earthquake Engineering* 1988; 7 (1): 22-31.
9. Luco JE, Wong HL. Forced vibration of Lotung containment model: theory and observations. *J of Engineering Mechanics* 1990; 116 (4): 845-861.
10. Luco JE, de Barros FCP. Identification of structural and soil properties from vibration tests of the Hualien containment model. *Earthquake Engineering & Structural Dynamics* 2005; 34: 21–48. DOI: 10.1002/eqe.404
11. Pitilakis D, Rovithis E, Anastasiadis A. Athanasios V, Manakou M, Field evidence of SSI from full-scale structure testing. *Soil Dynamics & Earthquake Engineering* 2018. 112, 89-106
12. Luco JE, Trifunac MD, Wong HL. Isolation of soil-structure interaction effects by full-scale forced vibration tests. *Earthquake Engineering & Structural Dynamics* 1988; 16 (1): 1-21.
13. de Barros FCP, Luco JE. Identification of foundation impedance functions and soil properties from vibration tests of the Hualien containment model. *Soil Dynamics & Earthquake Engineering* 1995; 14 (4): 229-248.
14. Tileylioglu S, Stewart JP, Nigbor RL. Dynamic stiffness and damping of a shallow foundation from forced vibration of a field test structure. *J of Geotechnical & Geoenvironmental Engineering* 2011; 137 (4): 344-353.

15. Star LM, Givens MJ, Nigbor RL, Stewart JP. Field-testing of structure on shallow foundation to evaluate soil-structure interaction effects. *Earthquake Spectra* 2015; 31 (4): 2511-2534.
16. NIST. Soil-structure interaction for building structures, Report No. NIST GCR 12-917-21, National Institute of Standards and Technology, U.S. Department of Commerce, Washington D.C. 2012.
17. American Society of Civil Engineers. Minimum design loads and associated criteria for buildings and other structures: ASCE/SEI 7-16. 2017.
18. Ljung L. *System Identification — Theory for the User, 2nd ed.* Upper Saddle River, N. J.: PTR Prentice Hall, 1999.
19. Lin CC, Wang JF, Tsai CH. Dynamic parameter identification for irregular buildings considering soil-structure interaction effects. *Earthquake Spectra* 2008; 24 (3): 641–666.
20. Wu WH, Wang JF, Lin CC. Systematic assessment of irregular building–soil interaction using efficient modal analysis. *Earthquake Engineering & Structural Dynamics* 2001; 30 (4): 573-594.
21. Hong AL, Betti R, Lin CC. Identification of dynamic models of a building structure using multiple earthquake records. *Structural Control & Health Monitoring* 2009; 16 (2), 178-199.
22. Pitilakis D, Lamprou D, Manakou M, Rovithis E, Anastasiadis A. System identification of soil-foundation structure systems by means of ambient noise records: the case of EuroProteas model structure in Euroseistest. *Proceedings of the 2nd European Conf. on Earthquake Engineering and Seismology*. Istanbul, Turkey, 2014.
23. Beck JL, Jennings PC. Structural identification using linear models and earthquake records. *Earthquake Engineering & Structural Dynamics* 1980; 8 (2), 145-160.
24. Papageorgiou AS, Lin BC. Analysis of recorded earthquake response and identification of a multi-story structure accounting for foundation interaction effects. *Soil Dynamics & Earthquake Engineering* 1991, 10 (1), 55-64.
25. Şafak E. Adaptive modeling, identification, and control of dynamic structural systems. I: Theory. *J of Engineering Mechanics* 1989; 115 (11), 2386-2405.
26. Şafak E. Adaptive modeling, identification, and control of dynamic structural systems. II: applications. *J of Engineering Mechanics* 1989; 115 (11), 2406-2426.
27. Şafak E, Çelebi M. Seismic response of Transamerica building. II: system identification. *J of Structural Engineering* 1991; 117 (8): 2405-2425.
28. Şafak E, Çelebi M. Recorded seismic response of Pacific Park Plaza. II: system identification. *J of Structural Engineering* 1992; 118 (6):1566-89.
29. Çelebi M. Recorded earthquake responses from the integrated seismic monitoring network of the Atwood Building, Anchorage, Alaska. *Earthquake Spectra* 2006; 22 (4), 847-864.
30. Chen Z, Trombetta NW, Hutchinson TC, Mason HB, Bray JD, Kutter BL. Seismic system identification using centrifuge-based soil-structure interaction test data. *J of Earthquake Engineering* 2013, 17 (4), 469-496.
31. Trombetta NW, Mason HB, Chen Z, Hutchinson TC, Bray JD, Kutter BL. Nonlinear dynamic foundation and frame structure response observed in geotechnical centrifuge experiments. *Soil Dynamics & Earthquake Engineering* 2013; 50, 117-133.
32. Şafak E. Detection and identification of SSI in buildings from vibration recordings, *J of Structural Engineering* 1995; 121 (5): 899-906.

33. Todorovska MI, and Trifunac MD. The system damping, the system frequency and the system response peak amplitudes during in-plane building-soil interaction. *Earthquake Engineering & Structural Dynamics* 1992; 21 (2): 127-144.
34. Moaveni B, He X, Conte JP, Restrepo JI, Panagiotou M. System identification study of a 7-story full-scale building slice tested on the UCSD-NEES shake table. *J of Structural Engineering* 2010; 137 (6): 705-17.
35. Asmussen JC. *Modal analysis based on the random decrement technique: application to civil engineering structures* [Doctoral dissertation]. Denmark: University of Aalborg; 1997.
36. Ghahari SF, Ghannad MA, Taciroglu E. Blind identification of soil–structure systems. *Soil Dynamics & Earthquake Engineering* 2013; 45: 56–69.
37. Ghahari SF, Abazarsa F, Avci O, Çelebi M, Taciroglu E. Blind identification of the Millikan Library from earthquake data considering soil–structure interaction. *Structural Control & Health Monitoring* 2016; 4 (23): 684-706. DOI: 10.1002/stc.180342
38. Taciroglu E, Ghahari SF, Abazarsa F. Efficient model updating of a multi-story frame and its foundation stiffness from earthquake records using a timoshenko beam model. *Soil Dynamics & Earthquake Engineering* 2017; 92: 25–35.
39. Skolnik D, Lei, Y, Yu, E, Wallace JW. Identification, model updating, and response prediction of an instrumented 15-story steel-frame building. *Earthquake Spectra* 2006; 22 (3): 781–802,
40. Beck JL. Bayesian system identification based on probability logic. *Structural Control & Health Monitoring* 2010; 17: 825–847. DOI: 10.1002/stc.424
41. Ho BL, Kalman RE. Effective construction of linear state-variable models from input-output functions. *Regelungstechnik* 1965; 12: 545–548.
42. Akaike H. Stochastic theory of minimal realization. *IEEE Trans. Automatic Control* 1974; 26: 667–673.
43. Van Overschee P, De Moor B. Continuous-time frequency domain subspace system identification. *Signal Processing* 1996; 52 (2):179-94.
44. Brincker R, Andersen P. Ambient response analysis of the Heritage Court Tower building structure. *Proceedings of the 18th International Modal Analysis Conference.* San Antonio, TX, 2000.
45. Peeters B, De Roeck G. Reference-Based Stochastic Subspace Identification for Output-Only Modal Analysis. *Mechanical Systems and Signal Processing* 1999; 13(6), 855-878.
46. Juang J, Papa RS. An eigensystem realization algorithm for modal parameter identification and model reduction. *Journal of Guidance, Control, & Dynamics* 1995; 8 (5): 620-627.
47. Phan M, Horta LG, Juang J, Longman RW. Identification of linear systems by an asymptotically stable observer. *NASA Tech. Paper, 3164* 1992.
48. Lus HI, Betti RA, Longman RW. Identification of linear structural systems using earthquake-induced vibration data. *Earthquake Engineering and Structural Dynamics* 1999; 28 (11): 1449-68.
49. James GH, Carne TG, Lauffer JP. The natural excitation technique (NExT) for modal parameter extraction from operating structures. *Modal Analysis-the International Journal of Analytical and Experimental Modal Analysis* 1995; 10 (4): 260-277
50. Juang J. System realization using information matrix, *J of Guidance, Control, and Dynamics* 1997; 20 (3): 492-500.

51. Jazwinski AH. *Stochastic Processes and Filtering Theory*, Academic Press, New York, N.Y., 1970.
52. Hoshiya M, Saito, E. Structural identification by extended Kalman filter. *J of Engineering Mechanics* 1984; 110 (12): 1757-1770.
53. De Callafon RA, Moaveni B, Conte JP, He X, Udd E. General realization algorithm for modal identification of linear dynamic systems. *J of Engineering Mechanics* 2008; 134 (9): 712-22.
54. Åström KJ, Bohlin T. Numerical identification of linear dynamic systems from normal operating records. *Proc. IFAC Symposium on Self-Adaptive Systems*. Teddington, UK. 1965.
55. Chopra AK. *Dynamics of structures, 4th Edition*, Prentice-Hall, Upper Saddle River, NJ, 2012.
56. Brincker R, Zhang L, Andersen P. Modal identification of output-only systems using frequency domain decomposition. *Smart Materials and Structures*. 2001; 10 (3): 441-445.
57. Ghahari SF, Abazarsa F, Ghannad MA, Taciroglu E. Response-only modal identification of structures using strong motion data. *Earthquake Engineering & Structural Dynamics* 2013; 42: 1221–12. DOI: 10.1002/eqe.2268
58. Ghahari SF, Abazarsa F, Ghannad MA, Çelebi M, Taciroglu E. Blind modal identification of structures from spatially sparse seismic response signals. *Structural Control Health Monitoring* 2014; 21 (5): 649–674. DOI: 10.1002/stc.1593
59. Crouse CB, McGuire J. Energy dissipation in soil-structure interaction. *Earthquake Spectra* 2001; 17: 235-259.
60. Crouse CB, Liang, GC, Martin, GR. Experimental study of soil-structure interaction at an accelerograph station. *Bulletin of the Seismological Society of America* 1984; **74**: 1995-2013.
61. Tileylioglu S. *Evaluation of soil-structure interaction effects from field performance data*. [Doctoral dissertation]. University of California, Los Angeles; 2008.
62. Veletsos AS, Meek JW. Dynamic behavior of building-foundation systems. *Earthquake Engineering & Structural Dynamics* 1974; 3 (2):121-38.
63. Givens MJ, Mylonakis G, Stewart JP. Modular analytical solutions for foundation damping in soil-structure interaction applications. *Earthquake Spectra.* 2016; 32 (3): 1749-68.
64. Pais A, Kausel E. Approximate formulas for dynamic stiffnesses of rigid foundations. *Soil Dynamics & Earthquake Engineering*. 1988; 7 (4): 213-227.
65. Stewart JP, Seed RB, Fenves GL. Empirical evaluation of inertial soil-structure interaction effects, Rpt. No. PEER-98/07, Pacific Earthquake Engineering Research Center, University of California, Berkeley, 205 pgs. 1998.
66. Stewart, JP, Seed RB, Fenves GL. Seismic soil-structure interaction in buildings. II: empirical findings, *J Geotech. & Geoenv. Engrg.* 1999; 125, 38-48.
67. Star LM. *Seismic vulnerability of structures: Demand characteristics and field testing to evaluate soil-structure interaction effects*. [Doctoral dissertation]. University of California, Los Angeles; 2011.
68. Givens MJ. *Dynamic soil-structure interaction of instrumented buildings and test structures.* [Doctoral dissertation]. University of California, Los Angeles; 2013.
69. Brandenberg SJ, Coe J, Nigbor RL, Tanksley K. Different approaches for measuring ground strains during pile driving at a buried archeological site. *J of Geotechnical & Geoenvironmental Engineering* 2009; 135 (8), 1101-1112.

70. Idriss IM, Sun JI. Users' manual for SHAKE91: A modified version of SHAKE for conducting equivalent linear seismic response analyses of horizontally layered soil deposits. Center for Geotechnical Modelling, University of California, Berkley, Calif. 1991.
71. Menq FY. *Dynamic properties of sandy and gravelly soils*. [Doctoral dissertation]. The University of Texas at Austin; 2003.
72. Darendeli MB. *Development of a new family of normalized modulus reduction and material damping curves*. [Doctoral dissertation]. The University of Texas at Austin; 2001.